Compressible and confined vortex flow

J. Wilkinson, A. Motamed-Amini, and I. Owen
Heat and Mass Transfer Laboratory, The Department of Mechanical Engineering,
The University of Liverpool, P.O. Box 147, Liverpool L69 3BX, UK

Accepted for publication February 1988

The internal compressible flow of a thin vortex chamber was investigated experimentally by measuring the radial distribution of temperature and pressure, from which the velocity field was calculated. The bulk of the internal vortex was found to be described by $u_\theta r^{0.69} = \text{constant}$. The total resistance of the vortex chamber to the flow was also investigated in the context of fluidic vortex diode behavior under conditions of compressible and choked flow. It was found that the vortex chamber choked at an upstream-to-downstream pressure ratio of about 6 and in doing so passed a mass flow rate of 28% of the equivalent one-dimensional ideal nozzle. The resistance of vortex chambers is known to be strongly influenced by the presence of reversed flow in the exit due to vortex breakdown. Schlieren photography of the swirling exhaust flow was used to show that, while vortex breakdown does occur, it can only do so after the flow has become subsonic downstream of the exit and cannot therefore influence the vortex chamber resistance.

Keywords: compressible vortex; confined vortex; vortex breakdown; power fluidics; vortex diodes; vortex throttles

Introduction

Compressible vortex flows are encountered in a number of different situations. In some of these (for example, spinning rockets, cyclone combustors, fluidic vortex valves, cyclone separators and wing tip vortices), sonic velocities may be reached in regions of the flow. The stimulus for the present work was provided by the observed behavior of fluidic vortex diodes when used with gases under conditions of compressible flow. Briefly, a vortex diode is a passive device located in a fluid circuit and which has the ability to offer a high resistance to the flow in one direction while offering minimal resistance when the flow is reversed. Examples of applications are as flow restrictors installed into gas-cooled nuclear reactor cooling circuits to prevent rapid depressurization in the event of a loss of coolant accident,[1] and as rectifying elements in fluidic diode pumps.[2] A feature of vortex diode behavior is that its high-resistance performance reduces as the flow through it becomes more compressible. Although the effects of compressibility in vortex devices have long been recognized,[1,3,4] they have not been investigated in any depth. To shed light on this and to help understand better the nature of confined compressible vortex flow, the work described in this paper was carried out with the support of the United Kingdom Atomic Energy Authority.

A sketch of the flow through a thin vortex chamber, such as that used in a vortex diode, is shown in Figure 1. In the present study the vortex chamber geometry was kept simple and lacked some of the refinement of standard vortex diodes.[1] Superheated steam was used as the working fluid, since this medium behaves much like an ideal gas and because it was exhausted into a subatmospheric condenser, relatively high pressure ratios could be achieved for modest inlet pressures.

The internal flow was investigated using the vortex chamber shown in Figure 2. The information gathered from this apparatus was used together with a simplified analysis of a spiral vortex to provide detailed information of the flow. Direct measurement of the vortex chamber velocity by pitot tube proved impossible as the probe significantly affected the vortex; a similar observation was made by Holman and Moore.[5] In addition to the measurements made in the steam flow using the vortex chamber described in Figure 2, a second, smaller, vortex chamber was manufactured and used with high-pressure air exhausting into the atmosphere so that Schlieren photography could be used to visualize the expanding swirling flow issuing from the exhaust port on the axis of the vortex chamber. This was of particular interest, since it is known that vortex valves derive their high-resistance capability not wholly from the pressure drop across the confined vortex, but more significantly from the aerodynamic blockage which occurs in the axial port as the swirling, expanding flow experiences vortex breakdown.[6]

Vortex theory

Mathematical models of circular flows can be derived based on combinations of forced vortex, free vortex, and sink flows. An assumption commonly assigned to confined vortex flow is that a forced vortex exists within the chamber exit radius where the fluid rotates as a solid body, being driven by a surrounding free vortex. Since this model assumes there is no radial component of velocity, the radial pressure gradient will be given

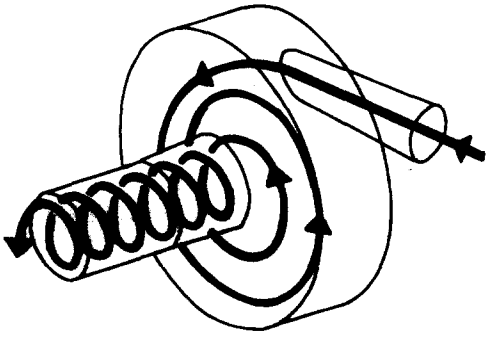

Figure 1 Flow through vortex chamber

by

$$\frac{\partial p}{\partial r}=\rho\frac{u_\theta^2}{r} \tag{1}$$

where u_θ is the tangential velocity component at radius r. The maximum tangential velocity occurs at the point of transition from free to forced vortex—this model being known as a "Rankine vortex."

An alternative model is a combination of free vortex and sink flow. This approach considers a radial flow component established by the strength of the sink. The region within the exit radius may be represented by a combination of forced vortex and sink flow. Axial flow is again ignored except at the exit port center to which the fluid converges uniformly and from which fluid is continuously removed.

The above models are idealistic representations of the flow regimes which may exist in a confined vortex. However, the dependence on Bernoulli's equation in the ensuing analyses restricts their application to incompressible flow.

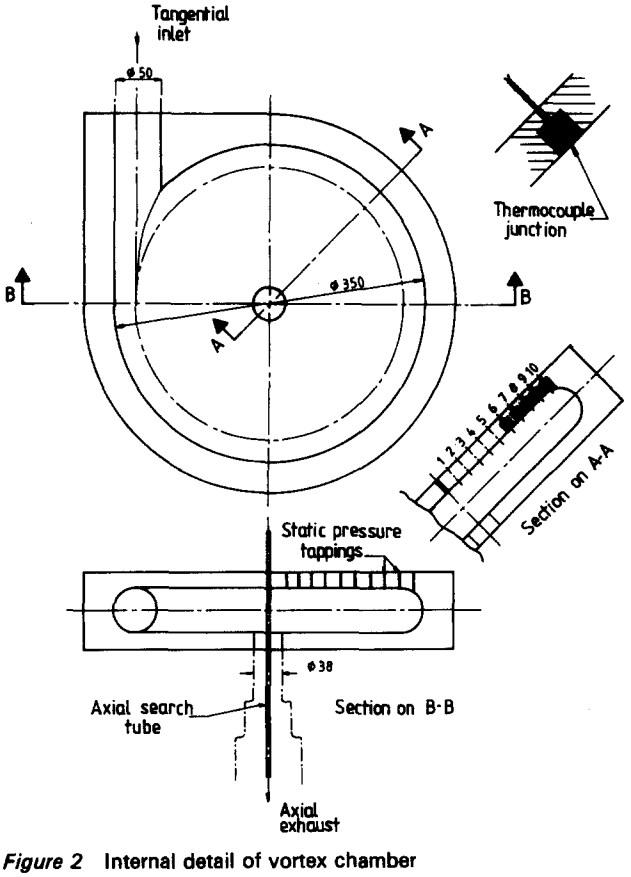

Figure 2 Internal detail of vortex chamber

The free vortex flow in the vortex chamber can be represented for a viscous and variable density flow by the Navier-Stokes equation of motion:

$$\rho\frac{DU}{Dt}=\rho g-\nabla p+\mu\nabla^2U+\tfrac{1}{3}\mu\nabla(\nabla\cdot U) \tag{2}$$

If this equation is cast in cylindrical coordinates, r, θ, z and we make the usual assumptions that the flow is frictionless and steady, then it reduces to a much simpler form. Another important assumption to be made is that the flow has a constant density. Although this assumption appears contradictory to the purpose of the present study, if, for now, it is allowed to stand, it will be referred to and discussed later in the light of experimental data.

Thus, Equation 2 finally reduces to

$$u_r\frac{\partial u_r}{\partial r}-\frac{u_\theta^2}{r}=-\frac{1}{\rho}\frac{\partial p}{\partial r} \tag{3}$$

from which the tangential velocity in the vortex may be found if the distribution of density ρ, radial velocity u_r, and static pressure p, are known. It can be seen that Equation 3 reduces to Equation 1 when u_r is neglected.

Experimental arrangement and procedure

The quantitative investigation was carried out using the vortex chamber installed in the characterization rig depicted in Figure 3. A gas-fired superheater provided thermostatic control of the steam supply. The vortex chamber and adjacent pipework were well insulated.

Superheated steam was deemed suitable for use in this investigation because it could be considered as an ideal gas. For the perfect gas laws to remain applicable, with constant isentropic index γ and gas constant R throughout the chamber, the degree of superheat was maintained sufficiently high to avoid saturation and phase-change effects.

The steam was supplied to the vortex chamber via isolation and pressure-reducing valves followed by a pair of throttle valves to regulate and finely adjust the upstream pressure P_u before admission to the vortex chamber tangential inlet port. The downstream pressure P_d was similarly controlled by a throttle valve exhausting into the subatmospheric condenser. This condensing, low-pressure compressible flow rig was designed to enable large upstream/downstream pressure ratios P_u/P_d to be obtained for modest inlet pressures. Upstream and

Notation

A	Area
C_f	A discharge factor
Cp	Specific heat at constant pressure
h	Vortex chamber height
k	Temperature recovery factor
$\dot{m}$	Mass flow rate
$\dot{m}_C$	Critical mass flow rate
M	Mach number
n	Vortex exponent
n_1	Index of polytropic expansion
p	Pressure
P_d	Downstream pressure
P_u	Upstream pressure
r	Radius
r_e	Exit port radius
R	Gas constant
T	Static temperature
T_0	Total temperature
T_u	Upstream temperature
u_θ	Tangential velocity
u_r	Radial velocity
x	Distance along exit duct
γ	Index of isentropic expansion
ρ	Density

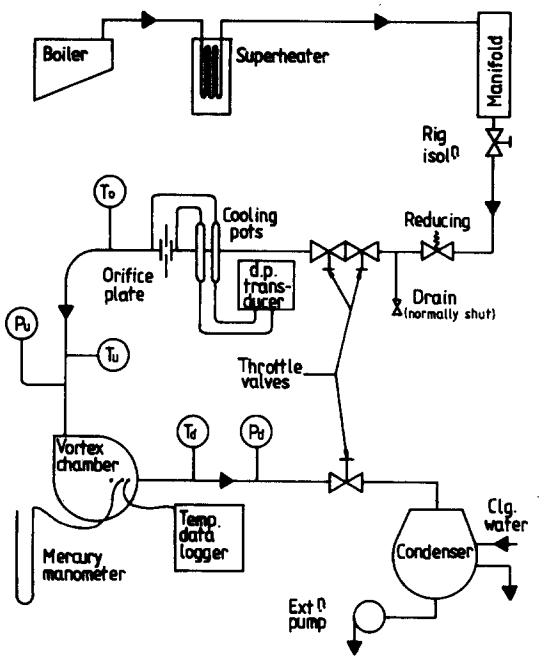

Figure 3 Arrangement of quantitative experimental rig

downstream conditions were measured by pressure gauges and half-shielded thermocouples, while an orifice plate was used to determine mass flow rate. From these readings the pressure-flow characteristics were obtained for a range of constant P_u. For each constant value of P_u, P_d was changed by throttling the flow into the condenser.

Instrumentation was also fitted directly to the vortex chamber to measure local static pressure and internal wall temperature. Ten static pressure tappings were drilled through the chamber wall, radially opposite the inlet port, as illustrated in Figure 2; also shown is a static pressure search tube fitted through a gland in the center of the chamber wall. This could slide along the axial center line to measure the static pressure through the exit duct and into the exhaust pipework. Individual radial or axial static pressures could then be recorded for constant inlet pressure and temperature using mercury U-tube manometers. The static pressure distribution through the vortex chamber was thus determined for varying upstream/downstream pressure ratios while maintaining a constant upstream pressure, which was manually controlled and carefully monitored by a water-flooded mercury manometer.

Ten internal surface temperature probes were fitted at 45° to the pressure tappings and at the same radii. These consisted of flush-mounted thermocouples in tufnol plugs bonded into flat-bottomed holes in the chamber internal wall, also shown in Figure 2. The purpose of the tufnol was to thermally insulate the thermocouples from possible temperature gradients due to conduction in the steel wall. Flush mounting was necessary to prevent disturbance of the flow under investigation and to record local surface temperature only, without disturbing the bulk flow.

A multichannel A/D converter controlled by a microcomputer was used to log the thermocouple temperature readings. The microcomputer was programmed to log both a running average of the temperature at each station and the standard deviation of the readings. Readings were taken at the same pressure ratios achieved in the pressure distribution investigation.

The qualitative investigation using air and Schlieren photography was carried out using a smaller vortex chamber with a 10-mm diameter exit. This vortex chamber was supplied with compressed air via a dome-loaded pressure controller and was arranged with the flow exhausting vertically upward into the laboratory. The exit port was set up centrally within the parallel field of view of Schlieren equipment. Compressed air was used for this investigation due to its plentiful availability and similar behavior to an ideal gas. Furthermore, using air allowed the exhaust flow to be examined as it discharged freely into the laboratory atmosphere. Instantaneous flow behavior was observed using a capacitor-discharged spark in an argon atmosphere as a light source. Such brief exposures were made in a darkened laboratory while holding open the camera shutter. Instantaneous exposures were made for inlet pressures increasing in increments of 1.72 bar (25 psig) up to 32.4 bar (470 psig).

Results and discussion

Overall pressure-flow characteristics

It was observed during the experiment that the state-points of the steam upstream and downstream of the vortex chamber were isenthalpic; this was to be expected, since neither external heat nor work transfers were present in the expansion process. The measured mass flow rate of steam, $\dot{m}$, was expressed non-dimensionally as a fraction of the mass flow $\dot{m}_C$ through a choked ideal isentropic nozzle having the same minimum area A as the vortex chamber (i.e., the throat diameter of the ideal nozzle was made equal to the exit port diameter of the vortex chamber). The resulting parameter C_f has been termed the "discharge factor," since it is only a true discharge coefficient in the choked region. Thus,

$$C_f = \frac{\dot{m}}{\dot{m}_C} \qquad \text{where } \dot{m}_C = \frac{AP_u}{\sqrt{T_u}}\left[\frac{\gamma}{R}\left(\frac{2}{\gamma+1}\right)^{(\gamma+1)/(\gamma-1)}\right]^{1/2} \tag{4}$$

In Figure 4 the discharge factor is shown as a function of inlet-to-outlet pressure ratio for different inlet pressures. The experimental points tend to fall onto one curve and show that the discharge factor is a function of pressure ratio up to about 6, above which a choking condition is reached.

This critical pressure ratio can be compared with a value of about 4 obtained in previous work by Owen and Motamed-Amini,[7] who used a vortex diode and which therefore had a different geometry from the present vortex chamber. Both values differ considerably from the theoretical value of 1.86 for one-dimensional isentropic flow. This can be attributed to the three-dimensional nature of the swirling flow in the throat, which

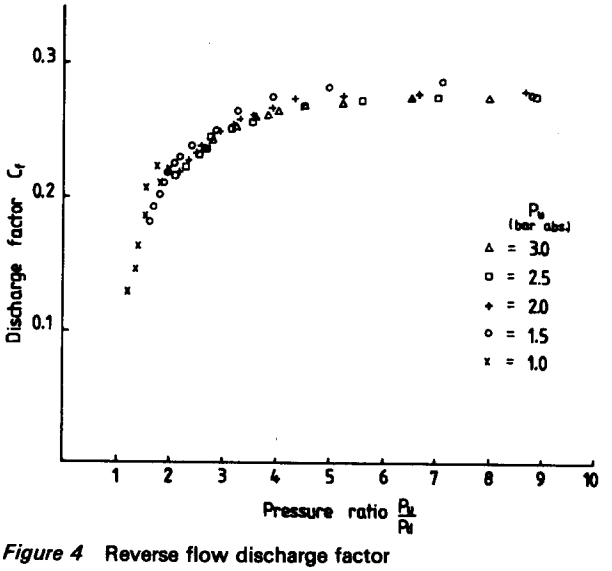

Figure 4 Reverse flow discharge factor

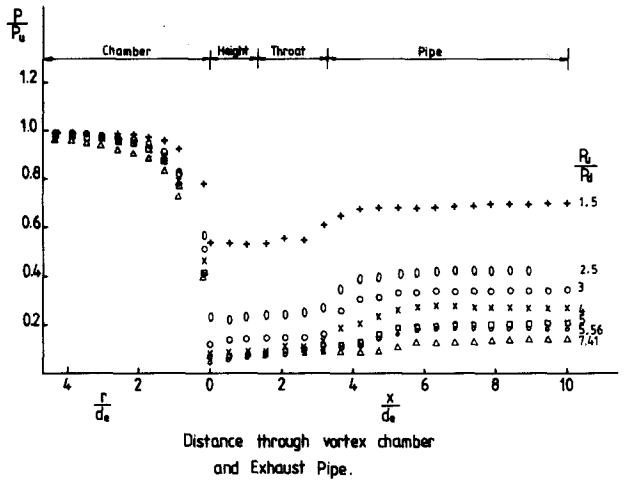

Figure 5 Static pressure distribution

will have both tangential and axial components. Transonic swirling flow was investigated by Lewellen *et al.*,[8] who indicated tangential Mach numbers as high as 1.4 may exist in the throat. Choking will be governed by the axial velocity component in the throat region. However, as pointed out by Lewellen *et al.*,[8] and discussed later in this paper in relation to vortex breakdown, the distribution of the axial component of velocity in swirling flow is not uniform across the duct. Choking will not, therefore, occur at a plane section, and the critical pressure ratio will be significantly higher than the one-dimensional isentropic value since it has to support both the axial and tangential components of velocity.

On Figure 4 an increase in C_f mostly represents a reduction in resistance to flow, which is seen to occur rapidly as the flow becomes compressible. This reduction in performance is a known characteristic of vortex diodes and reaches a constant as the flow becomes choked. In the choked region, $P_u/P_d > 6$, C_f approaches 0.28; i.e., the chamber exhausts only 28% of the ideal nozzle mass flow. This shows a greater resistance to flow than for a vortex diode, as presented by Owen and Motamed-Amini, where $C_f = 0.38$ for a similar pressure ratio. Although this represents a marked increase in resistance, it should be pointed out that a vortex diode is an optimized design to allow low resistance to flow in one direction as well as high resistance in the other. The chamber under investigation lacks the conical diffusers at the axial and tangential ports and the rounding of the tangential port entry associated with vortex diodes. Clearly the vortex chamber geometry is responsible for its improved flow resistance. This chamber is larger in diameter and wider than the aforementioned diode, so the effects of boundary layers on the vortex are less. Wormley[9] obtained the circulation distribution as a function of swirl ratio and established that the radial flow under high swirl conditions can be restricted to the chamber boundary layers. Thus the chamber design influences the flow in this region and can affect the flow regime in the rest of the chamber.

Internal flow

The static pressure distribution through the vortex chamber and exit pipe is illustrated in Figure 5 for various constant pressure ratios. Nondimensional static pressure readings are plotted against radial and axial tapping positions.

The pressure drop occurs mostly in the inner radii of the chamber near the throat. The pressure gradient steepens with increasing pressure ratio, and in all cases the lowest pressure is recorded on the axis at the chamber wall. This is supported essentially by the free and forced vortex combination model having a radial distribution with pressure reaching a minimum at the vortex center.

For subcritical cases (the lower pressure ratios) the pressure falls below P_d on the chamber axis and then experiences recovery by an adverse pressure gradient at the throat axis. This is not so apparent under fully choked conditions and suggests an "aerodynamic blockage" is present in the sub- and transonic range. As the pressure ratio is increased, the adverse gradient eases and appears to move downstream on choking. The concept of a reverse flow region, capable of restricting the main flow, is plausible, since such regions are known to exist where fluids are made to swirl and move axially through expanding cross sections. Much experimentation has been done by Gore and Ranz,[10] using air, and by Lewellen *et al.*[8] They investigated the pattern of swirling flows through a convergent-divergent nozzle as occurs in spinning rockets, cyclone separators, etc. They concluded that the observed reverse flow through the nozzle was incompatible with supersonic flow, which would explain the movement of the adverse pressure gradient downstream upon choking. They also found that supersonic flow appeared to be characterized by two recirculation zones: a recirculating internal cell within the chamber and an open cell downstream of the throat, as shown in Figure 6. The qualitative investigation showed some Schlieren photographic evidence of such external reverse flow regions.

As with velocity, the static temperature within the vortex chamber could only be measured by an instrument which would not disturb the flow. Fluid nearest the internal surface is brought to rest by viscous effects and, if the flow were adiabatic, would reach the stagnation temperature. However, velocity changes very quickly near the surface, and temperature gradients cause heat transfer within the boundary layer. Internal work is also done by shearing between adjacent fluid layers. Assuming an adiabatic wall, fluid in contact with the surface is at a temperature between the total and static temperatures, T_0 and T, due to some degree of temperature recovery through the boundary layer. The recovery factor k is given by

$$k = \frac{T_r - T}{T_0 - T} \qquad \text{where } 0.75 < k < 1$$

T_r is the local internal wall temperature, or recovery temperature, measured by thermocouples.

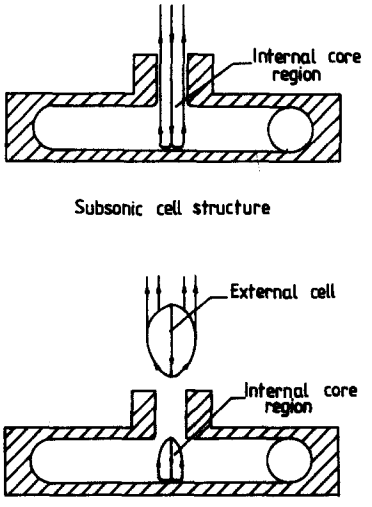

Figure 6 Position of recirculation zones

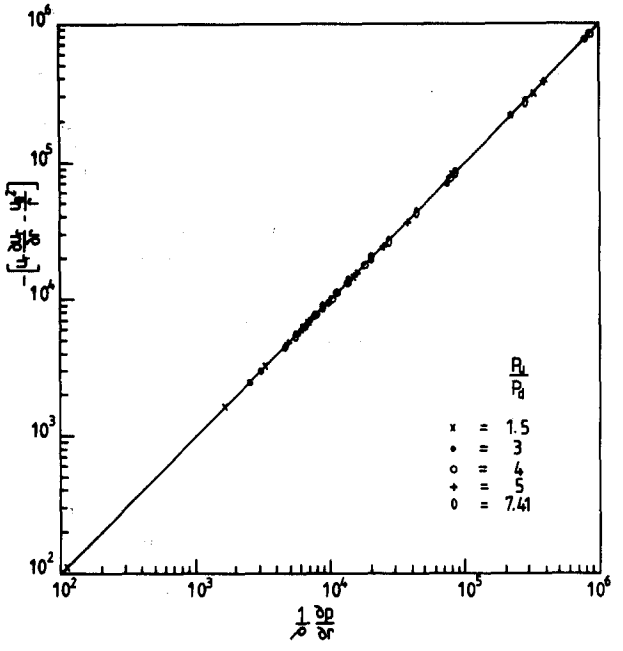

Figure 7 Validity of tangential velocity equation

Since static temperature and flow velocity are interrelated, a mathematical model of the vortex flow had to be chosen to provide another known variable. The combination of free and forced vortices assumes there is no radial velocity component and quotes the inviscid relation stated earlier:

$$\frac{dp}{dr}=\rho\frac{u_\theta^2}{r}$$

From this is derived

$$M=\left(\frac{r}{\gamma p}\frac{dp}{dr}\right)^{1/2} \tag{5}$$

which was used as a basis for an analysis of nitrogen flow by Kendall[11] and of air by Holman and Moore.[5] In the present work the Mach number relation was used to estimate static temperature by initially letting $k=1$; i.e., $T_0=T_r$ and $\gamma=1.335$. Then

$$T=\frac{T_r}{1+\frac{\gamma-1}{2}\left(\frac{r}{\gamma p}\frac{dp}{dr}\right)} \tag{6}$$

A convenient recovery factor is given by Emmons and Brainerd[12] as $k=\sqrt[3]{\mathrm{Pr}}$, $k\leqslant 1$. From the initial static temperature estimate, the Prandtl number was determined, enabling T to be recalculated. Radial velocity u_r was then found from continuity:

$$\dot{m}=\rho u_r 2\pi r h \tag{7}$$

where h is the height of the vortex chamber.

The tangential velocity was therefore calculated by Equation 1 using the measured pressure gradient, and the density, based on the static temperature, was calculated from Equation 6, and u_r by Equation 7.

Equation 1, however, neglects the radial component of velocity, although it is brought into account by consideration and systematic simplification of the Navier-Stokes equations of motion, as shown earlier:

$$u_r\frac{\partial u_r}{\partial r}-\frac{u_\theta^2}{r}=-\frac{1}{\rho}\frac{\partial p}{\partial r}$$

Recalling the earlier assumption of constant density, the above equation should only strictly apply for incompressible flow. However, when $u_r=0$, it does reduce to the earlier inviscid relation, which is valid for a compressible fluid vortex because, with purely tangential flow, constant density will exist along a streamline. Therefore to check the validity *with* radial velocity, experimentally derived values were inserted into the equation and the left and right sides compared, Figure 7. A straight-line correlation with unity slope is seen to exist. The variance about the line represents an error of $\pm 1.0\%$ in the application of this equation to compressible vortex flow. Thus, Equation 3 very adequately describes a compressible spiral vortex and emphasizes that the tangential component of velocity dominates the flow. Equation 1, and hence Equation 5, can therefore be used with confidence.

The velocity profiles have been plotted in terms of radial and tangential Mach numbers in Figures 8 and 9, respectively. As continuity predicts, the greatest increase in radial Mach number occurs within the inner radii of the chamber. The curves are not completed within the exit radius, since the radial velocity here will vary significantly across the chamber height as the flow takes on an axial component.

The tangential Mach numbers in Figure 9 are also seen to increase as the vortex is being driven toward the exit radius. The maximum tangential Mach number will probably peak at the inner instrumentation station. However, the complex three-dimensional velocity components within the exit radius could not be determined in this investigation.

To gain further information from the calculated results, the tangential velocity has been plotted against radius in Figure 10. If the flow was inviscid without chamber wall shear stresses restraining the vortex, the flow would be that of the free vortex,

$$u_\theta r^n=\text{constant} \qquad \text{where } n=1$$

since angular momentum must be conserved. The experimental data are therefore presented on a log plot to determine the degree to which they approximate the isentropic free vortex. The value of the vortex exponent n may be determined from the slope of the lines, which were established by the method of least squares. The lines in Figure 10 are relatively parallel, indicating that the vortex exponent is not too dependent on pressure ratio or mass flow rate. The average slope of the

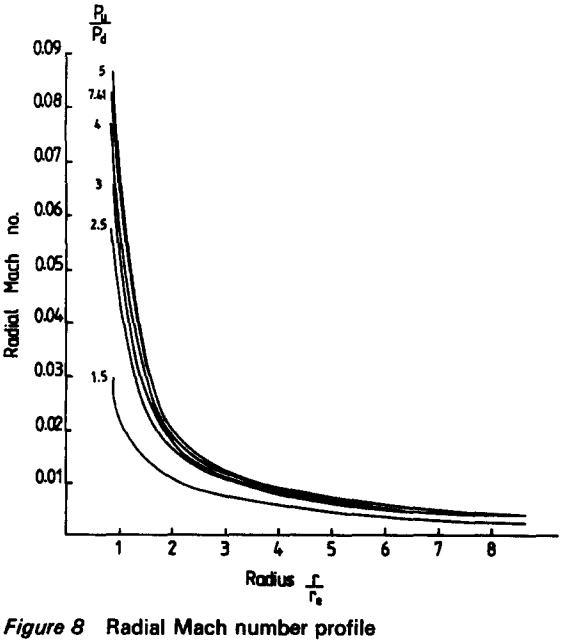

Figure 8 Radial Mach number profile

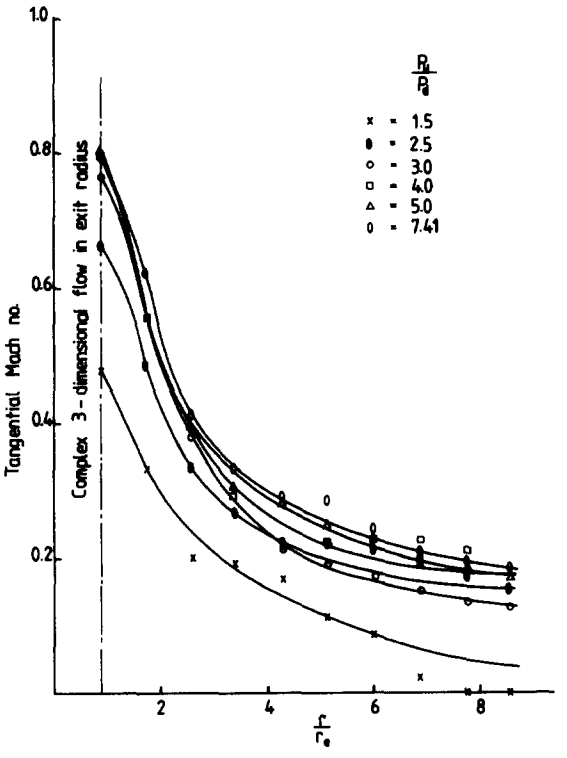

Figure 9 Tangential Mach number profile

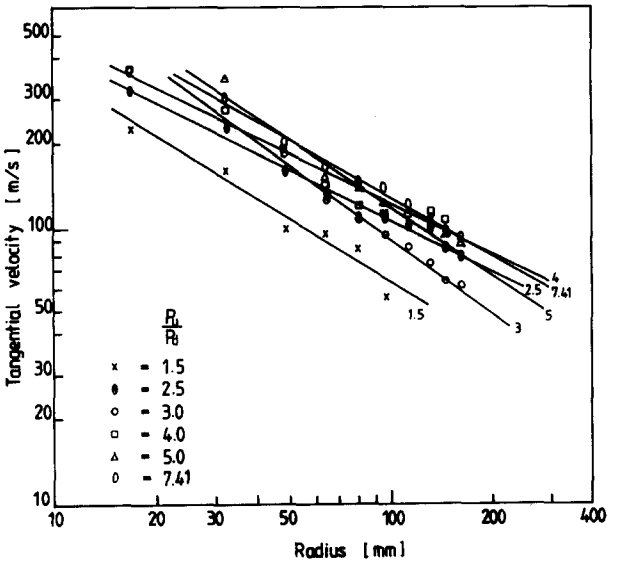

Figure 10 Determination of vortex exponent

straight lines was found to be 0.69, giving a general vortex relation of

$$u_\theta r^{0.69} = \text{constant}$$

determined from experimental readings of recovery temperature and static pressure. Since $n \neq 1$, the flow is not an isentropic free vortex.

The 10 thermocouple temperature readings showed very little variation across the chamber radius. With the exception of the inner two stations, the calculated values of static temperature remained greater than 120°C, giving $\mathrm{Pr} \geqslant 1$, and hence a recovery factor of 1. This then gives $T_0 = T_r$, which implies that the stagnation temperature T_0 remains essentially constant across most of the vortex, where the radial flow is very small. This confirms the assumption of constant stagnation temperature used by Holman and Moore[5] as a mathematical simplification to analyze velocity profiles from static pressures alone. They deduced a vortex exponent of 0.68 from a different analysis based on an energy balance, neglecting radial velocity. This correlates well with the exponent of 0.69 resulting from the analysis established in the present investigation.

The similarity of these values is noteworthy when considering their vortex chamber design (5-in diameter, 4 in long and 0.75-in exit diameter). Their analysis however did not apply well to a 2-in exit diameter chamber. Holman and Moore also presented an expression for the polytropic exponent n_1,

$$n_1 = \frac{1}{1 - nR/Cp}$$

where Cp is the specific heat of the gas at constant pressure. Substituting experimental values into this gives a polytropic exponent of 1.192 for the vortex chamber expansion. Comparing this with the isentropic index of $\gamma = 1.335$ again confirms a nonisentropic expansion process.

Compressible vortex breakdown

As stated earlier, the high resistance of vortex chambers operating with incompressible fluids is largely attributed to the blocking effect of strong reversed flows or backflows in the outlet throat. The initiation stages of an external backflow occur as rapid decelerations in a limited region, being known as "vortex breakdown." This can be defined as the stagnation of the axial flow followed by the occurrence of a region of reversed axial flow near the vortex centerline.

This concept is not compatible with choked and supersonic flows and was investigated by Lewellen *et al.*,[8] who proposed that in the subsonic case a backflow can exist from downstream of the exit, along the axis to the chamber wall. Then, by increasing the flow rate to transonic flow, the minimum cross section becomes choked and the backflow forms into two distinct cells as in Figure 6. Sarpkaya[13] observed this external cell as an ovoid region of circulating incompressible fluid. A similar flow structure in air is described by Gore and Ranz[10] as an almost spherical external recirculation zone with a clearly defined upstream stagnation point. This "bubble" type of vortex breakdown is described by Leibovitch[14] as looking like a body of revolution placed in the flow.

Another form is the "spiral" type appearing as a spiral shape rotating about the axis in the same sense as the fluid. A classic example of this phenomenon is its appearance in the leading edge vortex flows formed above a delta wing. In either form a stagnation point appears on the vortex axis followed by a limited region of reversed axial flow near the centerline. An expanding swirling flow such as that in the axial exit port of the vortex diode is known to cause vortex breakdown as a result of substantial swirl velocities increasing the pressure along the axis.

Hall[15] discussed in some detail the physical effects of compressibility on vortex cores. In particular, he considered the relative changes in the axial velocities at the centerline and at the core boundary. When a fluid with strong swirl enters a duct, there exists a steep radial pressure gradient with the minimum pressure on the centerline, as described by Equation 1. As the flow proceeds downstream, the swirl decays due to viscous effects, and as the level of the swirl reduces, so too does the radial pressure gradient. The result of this in the axial direction is that the difference in the upstream and downstream pressures is greater toward the wall than at the centerline. Coupled with the wall boundary layer this produces an axial velocity profile

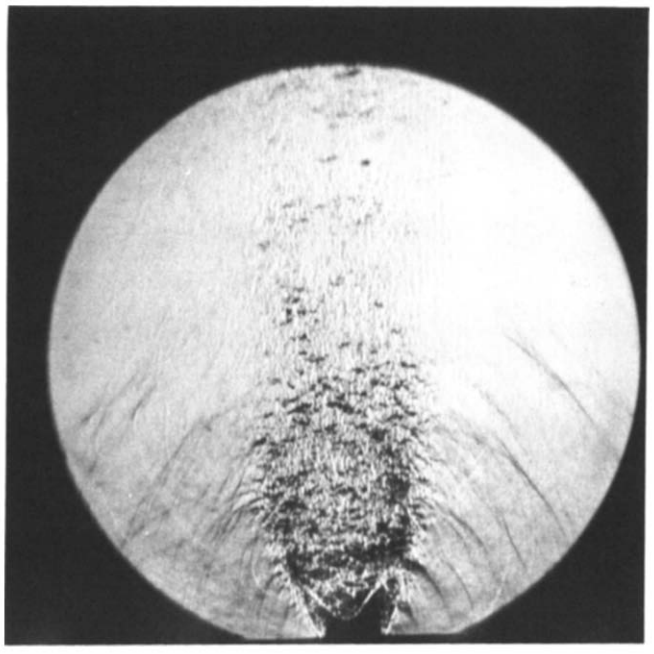

Figure 11 Schlieren photograph of compressible swirling exhaust flow ($P_u/P_d \sim 25$)

symmetrical around the axis of the duct with a peak toward the wall and a lower velocity region at the centerline.

When an incompressible flow such as that described above reaches an expansion, the axial velocity reduces. The centerline velocity, being lower than at the core boundary, will stagnate and then reverse—vortex breakdown will have occurred and a reverse flow zone will have formed. However, for an expanding supersonic flow, although the centerline axial velocity will again be less than that at the core boundary, both will be increasing—stagnation and flow reversal will not occur.

If this concept is now related to the swirling flow exhausting from the vortex chamber, then over some region in the exit duct the flow will choke when the axial Mach number reaches unity. (Clearly from the present discussion this will not occur at a plane section.) After this region the flow will accelerate and the axial velocity profile described above will be produced. The crude nozzle design ensures that the jet is underexpanded as it leaves the vortex chamber and the flow will encounter a complex shock wave and become subsonic. The conditions necessary for vortex breakdown have already been established in the supersonic region, and thus flow reversal will occur very soon after the shock wave. In relation to the vortex diode, therefore, a reverse flow zone will exist, but it will be downstream of the exit port and will have no influence on the diode resistance—hence the reduction in performance of the diode in going from conditions of incompressible to compressible flow.

Figure 11 shows a Schlieren photograph of the swirling exhaust flow. The flow is clearly highly turbulent and three-dimensional; this is the reason for the lack of clarity in the photographs and, despite much care, clearer images could not be obtained. The inlet pressure for Figure 11 was 25.5 bar ($P_u/P_d \sim 25$). The image shows a curved shock downstream of the exit after which an ovoid recirculation zone can be seen, which is followed by a turbulent wake. As the pressure ratio across the device was increased from the sub- to the supercritical range so the shock was seen to form at the exit and move downstream. The Schlieren images recording that sequence, while being discernible to the eye, were of poor quality (due to the swirling nature of the flow) and have not been reproduced herein.

The curved shock emphasizes the fact that the flow does not choke at a plane section. To reach stagnation conditions, the flow first becomes subsonic through the shock before decelerating rapidly into vortex breakdown. The exit port in the photograph forms an underexpanding nozzle, having no diverging portion at all. The shape of the shock wave in the expanding swirling jet forms an ideal geometry after which a "bubble"-type vortex breakdown may form. Figure 11 also clearly illustrates the radiation of sound waves from the source at the nozzle exit. This phenomenon was investigated in depth by Davies and Oldfield.[16]

Conclusions

The effect of compressibility on the operating characteristics of a fluidic vortex valve is to impair its high-resistance capability. This feature has been explained in the present work by investigating the flow through a thin vortex chamber using both steam and air. The internal flow of the vortex chamber produces a vortex described by $u_\theta r^{0.69} = \text{constant}$.

The vortex exponent compares well with work by Holman and Moore,[5] who used a vortex chamber with a much greater chamber height. The general form of the vortex appears therefore to be relatively independent of the chamber height, a somewhat surprising result since, intuitively, the wall shear would be expected to impose a greater influence on the flow in the thinner chamber. The polytropic index of the expansion for the steam flow in the vortex was found to be 1.192, compared with the isentropic value of 1.335.

The vortex chamber was found to choke at an inlet-to-outlet pressure ratio of about 6 and passed about 28% of the mass flow of the equivalent ideal one-dimensional nozzle. The corresponding values measured for a vortex diode by Owen and Motamed-Amini[7] were 4 and 38%. Clearly these values *are* influenced by the geometry of the vortex device.

The reduction in vortex chamber resistance as the flow becomes compressible has been considered through a discussion of vortex breakdown in expanding swirling flows, such as those found in the exit port of the vortex chamber. The discussion has been supported by Schlieren photography of the flow field in the exit region. It has been concluded that the aerodynamic blockage, which is largely responsible for the high resistance, is swept out of the axial port as the flow becomes compressible. This view is further supported by measurements of the static pressure along the centerline of the exit.

Acknowledgments

The authors wish to acknowledge the financial support of the United Kingdom Atomic Energy Authority.

References

1 Syred, N. and Roberts, P. J. Use of vortex diodes applied to post-accident heat removal systems. *ASME*, 1979, Paper 79-HT-9

2 Roberts, P. J. and Syred, N. Fluidic two diode pump system for hot and cold liquids. *Fluidics Quarterly*, 1978, **10**(3), 49–65

3 Syred, N. A vortex valve ejector combination for fluidic two-diode pumps. In Proc. Symp. Power Fluidics, Inst. Meas. & Control, 1975, London, Paper 1

4 George, P. J., Ward, J. R., and Mitchell, F. M. Vortex diode characteristics at high pressure ratios. In Proc. Symp. Power Fluidics, Inst. Meas. & Control, 1975, London, Paper 23

5 Holman, J. P. and Moore, G. D. An experimental study of vortex chamber flow. *J. Basic Eng. Trans. ASME*, 1961, Dec., 632–636
6 King, C. F. and Syred, N. An investigation of vortex phenomena associated with the axial flow reversal in high Reynolds number confined flow. In Proc. Session on Confined Vortex Flows, ASME Winter Annual Meeting, 1980, Chicago, 101–111
7 Owen, I. and Motamed-Amini, A. Compressible flow characteristics of a vortex diode operating with superheated steam. *ASME*, 1986, Paper 86-WA/FE-5
8 Lewellen, W. S., Burns, W. J., and Strickland, H. J. Transonic swirling flow. *AIAA J.*, 1979, 7(7), 1290–1297
9 Wormley, D. An analytical model for the incompressible flow in short vortex chambers. *J. Basic Eng. Trans. ASME*, 1969, June, 264–276
10 Gore, R. W. and Ranz, W. E. Backflow in rotating fluids moving axially through expanding cross sections. *AIChJ.*, 1964, **19**, 83–88
11 Kendall, J. M. Experimental study of a compressible viscous vortex. JPL Technical Report 32-290, June, 1962
12 Emmons, H. W. and Brainerd, J. G. Temperature effects in a laminar compressible fluid boundary layer along a flat plate. *Trans. ASME*, 1941, **63**, A-105
13 Sarpkaya, T. Vortex breakdown in swirling conical flows. *AIAA J.*, 1971, **9**, 1792–1799
14 Leibovitch, S. Vortex stability and breakdown: Survey and extension. *AIAA J.*, 1984, **22**(9), 1192–1206
15 Hall, N. C. The structure of concentrated vortex cores. *Progress in Aeronautical Science*, 1966, **7**, 53–110
16 Davies M. G. and Oldfield, D. E. S. Tones from a choked axisymmetric jet. I. Cell structure, eddy velocity, and source locations. *Acustica*, 1962, **12**(4), 257–267